Engineering Geology 187 (2015) 135–142

Contents lists available at ScienceDirect

Engineering Geology

journal homepage: www.elsevier.com/locate/enggeo

Stochastic fracture generation accounting for the stratification orientation in a folded environment based on an implicit geological model

Andrea Borghi *, Philippe Renard, Louis Fournier, François Negro

University of Neuchâtel, Center For Hydrogeology and Geothermics (CHYN), 11 Rue Emile Argand, 2000 Neuchâtel, Switzerland

ARTICLE INFO

Article history:
Received 30 July 2013
Received in revised form 17 November 2014
Accepted 25 December 2014
Available online 10 January 2015

Keywords:
Geological modeling
Discrete fracture network (DFN)
Stochastic modeling
Structural geology

ABSTRACT

This paper presents a new approach in generating stochastic discrete fracture networks. The particularity of the approach is that it allows us to simulate the theoretical families of fractures that are expected in a folded environment. The approach produces fractures that are consistent with the local stratigraphic orientation. The fractures are modeled as simple rectangular planar objects. When they are modeled, they are rotated according to the local stratigraphic orientation. As the stratigraphy is modeled using an implicit approach, we use the gradient of this geological potential field to retrieve the information about the geological orientation. The fracture number and size are following user-defined probability density functions.

1. Introduction

Fractures are very common objects in geological systems. These fractures have a significant impact on mechanical, geophysical and hydraulic properties of the rocks. The study of fractured systems is of great importance in many domains: petroleum industry, hydrogeology, waste disposal, geothermics, civil engineering (tunnels, dam stability).

Fractured systems have been studied by many authors, and the relationship between fracture orientation and folds has been underlined (Price, 1966; Price and Cosgrove, 1990; Twiss and Moores, 1992; Bazagette, 2004; Bellahsen et al., 2006; Zahm and Hennings, 2009). There are several parameters that must be taken into account to model correctly a fracture network such as density, size, and shape of the fractures. Until now, no simple general model has been commonly accepted, mainly due to the complexity of geological systems.

A wide literature exists about discrete fracture network (DFN) modeling, and several reviews have been published (Chilès, 2005; Dershowitz et al., 2004; Jing, 2003; Sassi et al., 2012). DFN can be used for a very wide range of applications. Here, the technique was developed as an initial step to model the formation of karstic systems in complex three dimensional folded environments (Borghi et al., 2012), but it could be directly applied for other problems. In general, the fracture objects in the DFN models are assumed to be planar (often rectangular or elliptic). For example, \Kloppenburg et al. (2003) use the results of a regional/local strain analysis[1] from borehole data to infer the orientation and density of fractures according to the probable deformation chronology. Freudenreich et al. (2005) use 3D maps of orientation and density derived from seismic observations. Other authors use geomechanical models in which the fractures grow during the deformation process, and the complex interactions between them – truncation of fracture sets against each other, already existing fractures damage zone and shadow zone (Olson, 1993) – can be modeled (Maerten et al., 2000), but these models are very difficult to condition by field observations, and need high computational resources. More recently, hybrid (combined stochastic and geomechanical) models have been proposed (Mace, 2006), as well as *pseudo-genetic* models (Bonneau et al., 2013; Davy et al., 2013). These techniques mimic the complex interactions between fractures without solving all the complexity of the fracturing physics.

There are less methodologies allowing to consider (and model) the variation of fracture orientation according to the orientation of the geological structures (dip and strike of the geological formations). This paper describes a methodology that can be used to generate a stochastic discrete fracture network (DFN), in which the fracture orientations are consistent with the orientation (deformation) of the geological formations.

The fracture generator presented in this paper is called *FRAGILe*, which stands for: *FRActure Generator based on an Implicit geomodeL*. The proposed methodology considers DFN composed by very simple fracture objects, i.e., the fractures are supposed to be rectangular. These fractures are modeled in folded sedimentary environments. The resulting DFN is generated according to the local orientation of the stratification. This is possible since the orientation map is extracted from an

* Corresponding author.
E-mail address: andrea.borghi@unine.ch (A. Borghi).

[1] Priest (1993) describes how to perform these strain analyses.

http://dx.doi.org/10.1016/j.enggeo.2014.12.019
0013-7952/

implicit geological model. In implicit geological modeling, the geology is not modeled as a multitude of distinct surfaces, but as iso-values of one or several continuous scalar fields. The proposed methodology uses the potential field method (Lajaunie et al., 1997; Moyen et al., 2004; Cowan et al., 2003; Frank et al., 2007; Calcagno et al., 2008; Caumon et al., 2013; Souche et al., 2013) to model the geological implicit function (Section 2.2).

The methodology described in the present paper considers that the potential field is known. It is assumed that the orientation of the fractures will follow a conceptual model such as the one described by Price and Cosgrove (1990) or Twiss and Moores (1992) (Section 2.4.1). The algorithm generates several sets of fractures (Section 2.4) that are rotated into the folded geological model according to the orientation of the stratigraphy (Section 2.5).

2. Detailed description of the modeling method

In this section, we describe the methodology that we use to generate the fractures. The generator is based on a stochastic approach, the dimensions and locations of the fractures are generated randomly. The

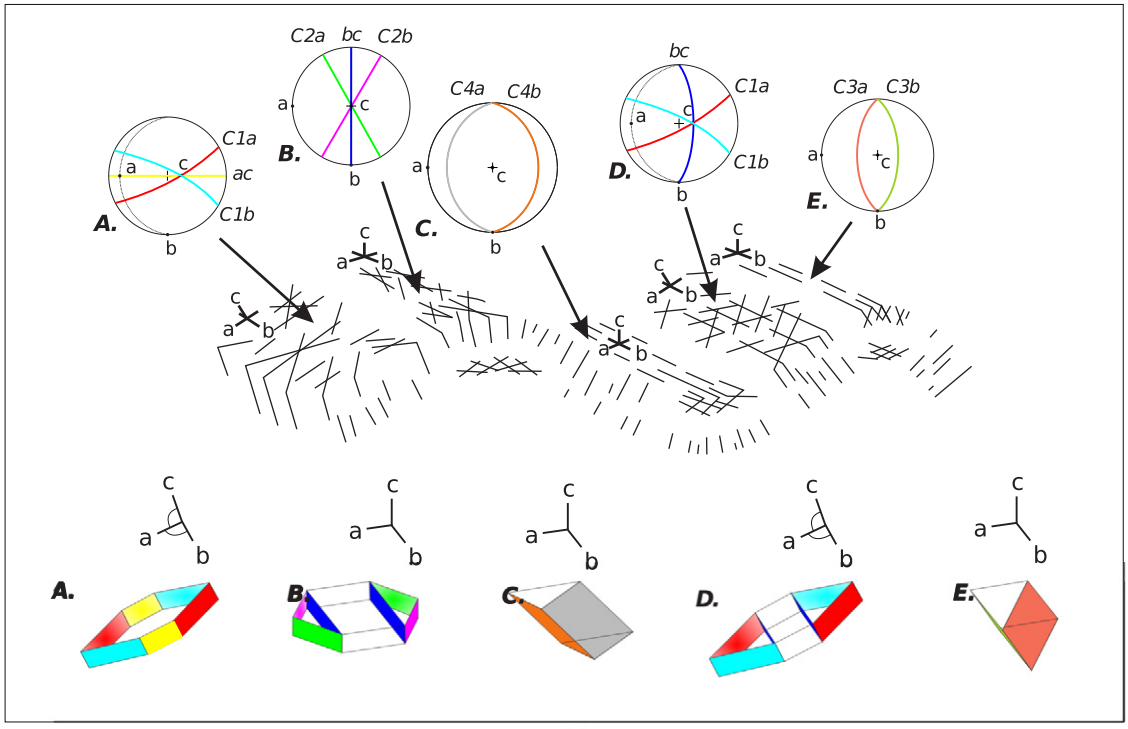

(a)

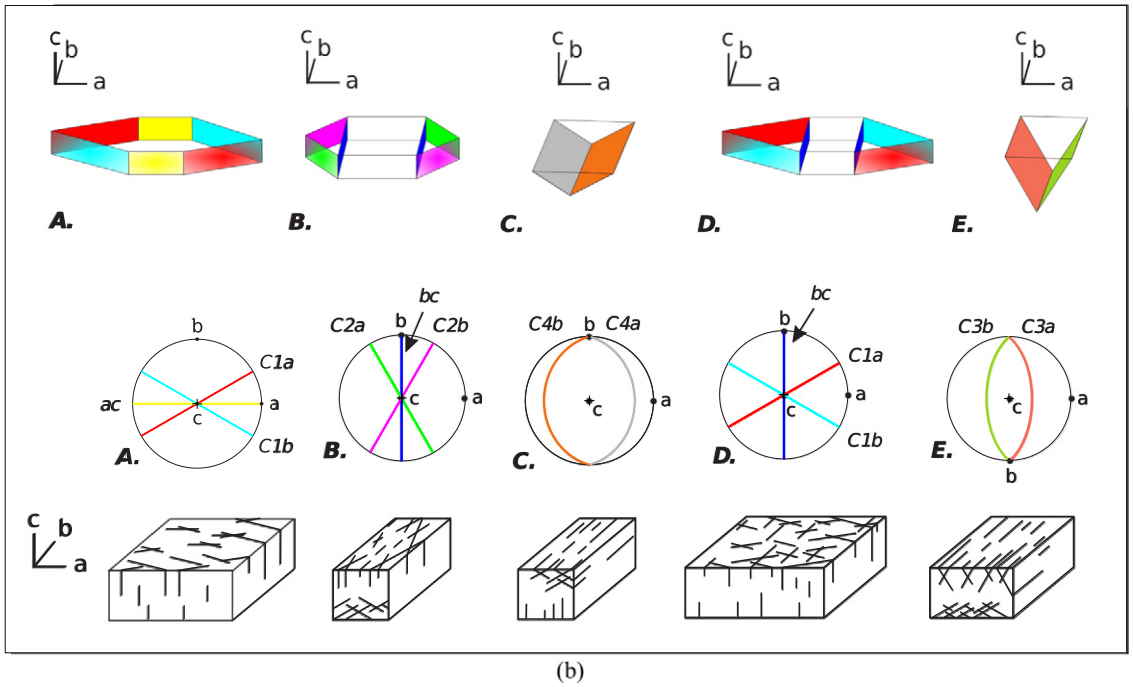

(b)

Fig. A.1. Illustration of the fracture sets in: a) folded environment (modified from Twiss and Moores, 1992), with conceptual plot and stereonets of fractures families (Schmidt lower hemisphere); b) in a reference environment (see Section 2.4.3). The colors are only meant to identify easily the families in the stereoplots.

probability distribution function (PDF) for the generation of fracture orientation must be defined by the user. The method allows us to use a combination of purely theoretical families of fractures, and families based on field observations.

The generation of the fractures is divided into 3 main steps:

- definition of the number and length of the fractures (Section 2.3)
- construction of the unrotated fractures (Section 2.4)
- positioning of the fractures into the geological model and rotation according to the local orientation of the structure (Section 2.5)

2.1. Conventions for geological surfaces

Geological surfaces (fractures or bedding planes) can be described using different terminology conventions. To avoid any ambiguity, the conventions that are used in this paper are the following:

- *strike*: orientation of the intersection between the geological plane and the horizontal plane, given in degrees (0 to 360) clockwise to the North.
- *dip*: angle between the geological plane and the horizontal plane, expressed in degrees (0 to 90). The strike is oriented so that the dip plunges on the right-hand side.
- *orientation*: normal vector to the geological plane.

2.2. Implicit geological model

The information of the orientation of the strata is extracted from an implicit geological model. In this work, we used the software *geomodeller* (Geomodeller3D, 2013) to compute the potential field; the resulting geological model is exported on a regular mesh, which contains the information about lithology type and orientation for every voxel.

We give here a very brief explanation of the implicit geological model that we use because some symbols defined here will be used later in the paper. The implicit approach is based on a potential field P defined over the model domain $\boldsymbol{\Omega} \in R^3$. This potential field $P(\boldsymbol{x}) \; \forall \; \boldsymbol{x} \in \boldsymbol{\Omega}$, is a scalar function defined for each point $\boldsymbol{x}$ of the domain. It is interpolated by cokriging two types of data: observed positions of geological interfaces and structural measurements (dip and strike) taken anywhere in the domain. The details of the method are described in Lajaunie et al. (1997) and Calcagno et al. (2008).

All the points having the same value of the potential $P(\boldsymbol{x_j})$ belong to the same geological interface. The orientation of the interface is given by the gradient of the potential $\boldsymbol{G}(\boldsymbol{x_j})$ which is the normal vector of the geological interface.

$$\boldsymbol{G}(\boldsymbol{x}) = \begin{bmatrix} G_x(x) \\ G_y(x) \\ G_z(x) \end{bmatrix} = \begin{bmatrix} \frac{\partial P}{\partial x}(\boldsymbol{x}) \\ \frac{\partial P}{\partial y}(\boldsymbol{x}) \\ \frac{\partial P}{\partial z}(\boldsymbol{x}) \end{bmatrix}. \quad (1)$$

Knowing the potential and its gradient allows defining for any point in the domain the geological formation and the orientation of the layers at that location.

2.3. Fracture size and density

One of the most difficult parameters to measure in the field, and subsequently to model, is the fracture length distribution. Many statistical models for the fracture length (negative exponential, uniform, normal, log-normal, power law, etc.) are commonly used in the literature (Priest and Hudson, 1981; La Pointe and Hudson, 1985; Priest, 1993). Many statistical studies show that exponential or power laws are often appropriate (Odling, 1997; Ackermann et al., 2001; Bour et al., 2002; Soliva and Benedicto, 2005; Davy et al., 2010).

In the proposed methodology, the user is free to choose the probability density distribution (PDF) for the fracture length that best suits his field observation for his own application. The discussion about the benefits and shortcoming of the different distributions is beyond the scope of the present paper.

Furthermore, the fractures are supposed to be rectangular. Their width d is proportional to the fracture length l. The shape ratio d/l is prescribed by the user as a constant or as PDF.

Similarly, the fracture density is assumed to be constant in this paper: the user defines a point density and the fracture centroids are computed following a Poisson point process. Note that the user defined density is not the fracture density but only the density of the centroids.

All these parameters can be defined for each fracture family if needed.

2.4. Construction of the fracture sets

2.4.1. Conceptual model

In our model, we can use either user defined fracture families (based on field observations, see 5) or, and this is the main novelty, the theoretical families of fractures that should be present in a fold, as proposed by Twiss and Moores (1992). This conceptual model suggests that six main fracture sets occur depending on the position within the fold. Fig. A.1a shows such fracture families. Even if this is only a conceptual representation of natural systems, it provides some guidelines for the definition of theoretical fracture sets, which are often observed in the field. The model includes 6 main families of fractures:

- Conjugate system C1: This system is roughly perpendicular to the fold axis: 2 conjugate high angle fracture systems (C1a and C1b) (situations A and D in Fig. A.1a.).
- Conjugate system C2: This system is roughly parallel to the fold axis: 2 subvertical conjugate fracture systems (C2a and C2b) (situation B in Fig. A.1a).
- Conjugate system C3: This system is parallel to the fold axis: 2 high angle conjugate fracture systems (C3a and C3b) (situation E in Fig. A.1a).
- Conjugate system C4: This system is parallel to the fold axis: 2 low angle conjugate fracture systems (C4a and C4b) (situation C in Fig. A.1a).
- Fractures with ac orientation: Vertical fractures that have their strike perpendicular to the fold axis (situation A in Fig. A.1a).

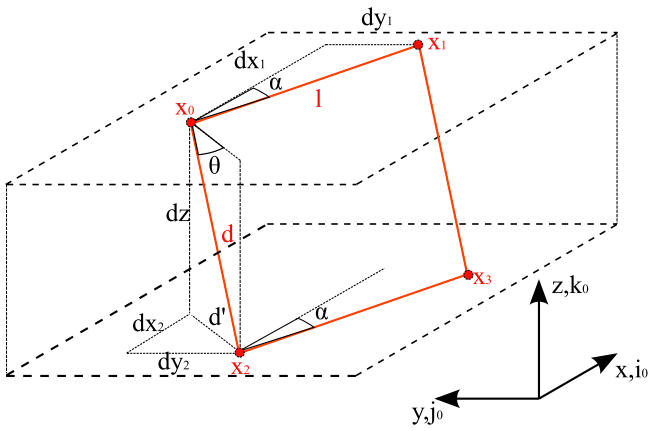

Fig. A.2. The 4 initial points of the basic "fracture object", x_i with $i \in [0, 3]$, see the text in Section 2.4.3. Symbols: $\boldsymbol{x}_{[0,3]}$ are the 4 points describing the fracture. dx_1 and dy_1 are the components of vector $\overrightarrow{\boldsymbol{x}_0\boldsymbol{x}_1}$, dz, dx_2 and dy_2 are the components of vector $\overrightarrow{\boldsymbol{x}_0\boldsymbol{x}_2}$, d' is the norm of vector $\overrightarrow{dx_2dy_2}$, α is the strike of the fracture, expressed in degrees from the x axis (trigonometric), θ is the dip of the fracture expressed in degrees.

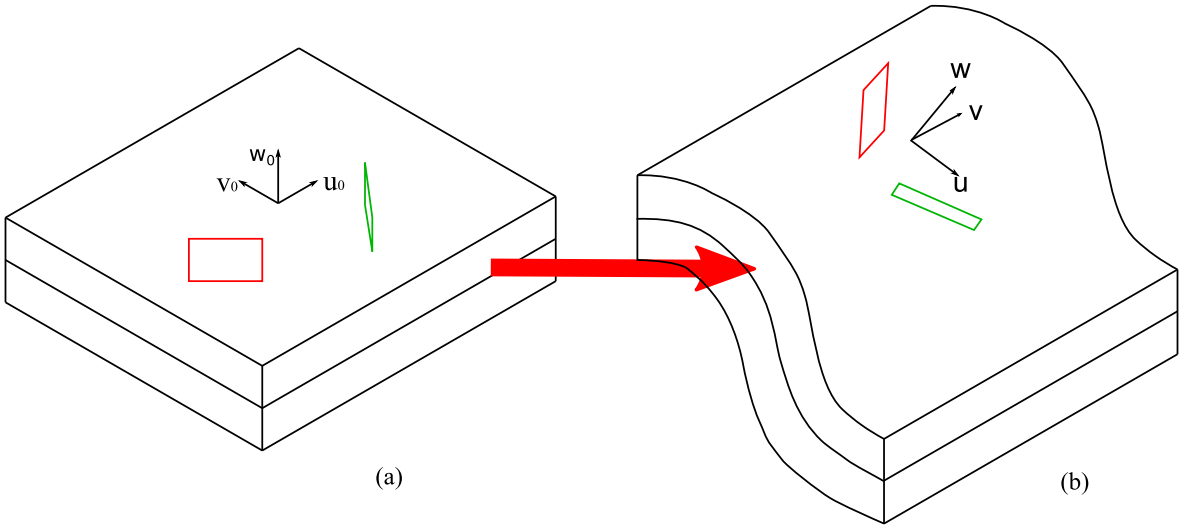

Fig. A.3. The original fractures (green and red objects) are first generated in an reference environment (a) and secondly rotated according to the local geological orientation (b), this is equivalent to a basis transformation from the initial (i_0, j_0, k_0) basis to the local (i,j,k) basis.

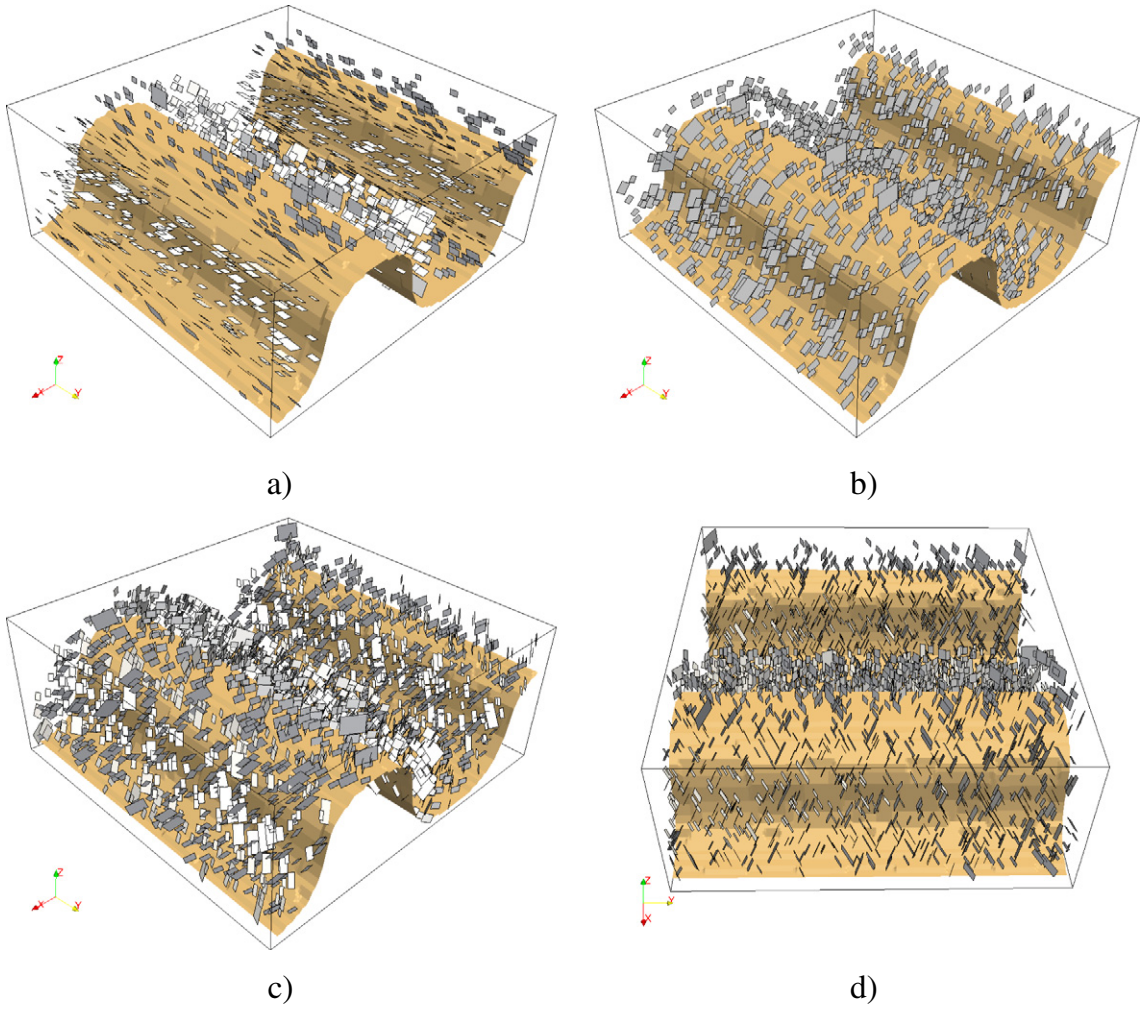

Fig. A.4. Rotated fractures according to the geological orientation. a) Fractures parallel to the fold axis, b) fractures perpendicular to fold axis, c) and d) two different view angles of two conjugate fracture families. NB: the brown surface represents the base of the formation.

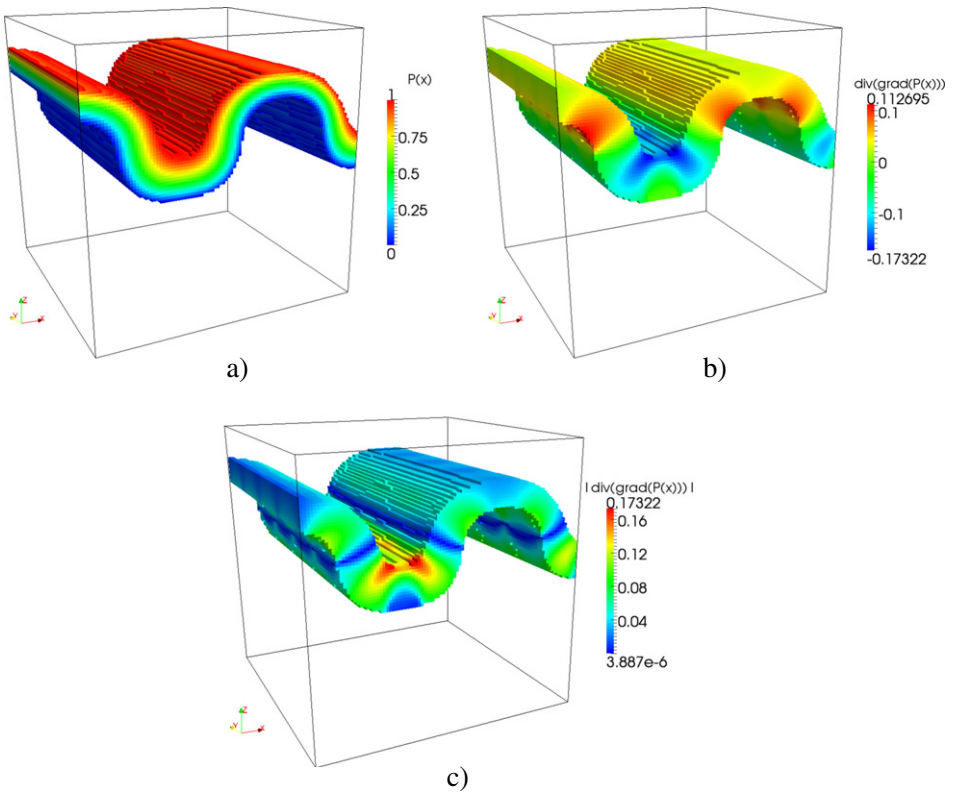

Fig. A.5. a) Normalized potential P'_f in one formation, b) Laplacian of the potential $\Delta \boldsymbol{G}(\boldsymbol{x})$, c) absolute value of the Laplacian ($|\Delta \boldsymbol{G}(\boldsymbol{x})|$). values.

- Fractures with bc orientation: High angle fractures with a strike parallel to the fold axis (situation B in Fig. A.1a).

The fracture systems C1 and ac are typical for fold limbs. The systems C2, C3 and bc are typical for the fold extrados (extension), while the system C4 is characteristic for the fold intrados (compression).

Fig. A.1b shows the families in a reference environment, i.e., in the environment that will be used do generate them as explained in the following sections.

2.4.2. Strike and dip probability distribution function definition

Each of the fracture sets described above are given for a theoretical case. In practice, the fractures are never perfectly parallel between them. Therefore in our approach, for every family the user has to define a PDF. In the case of a uniform distribution, upper and lower bound values for both strike and dip have to be provided, and in the case of a normal distribution, the mean value and standard deviation have to be provided. When each fracture composing the initial set is built, a random value of dip and strike is retrieved from the PDF of the family which the fracture belongs to.

2.4.3. Initial coordinates of the fracture vertices

Each initial fracture is generated after its length and its orientation information have been defined. As shown in Fig. A.2, the fractures are rectangular, and their initial vertices (the 4 corners of the fracture) are computed. Their length on the horizontal plane l is given by the chosen distribution (Section 2.3), and their width in the dip direction is given by $d = a * l$, with a being a user-defined (or random) ratio (Section 2.4.1). The vertex coordinates $\boldsymbol{x}_i$ with $i \in [0, 3]$ are:

$$\boldsymbol{x}_i = \boldsymbol{x}_0 + \overrightarrow{\boldsymbol{x}_0 \boldsymbol{x}_i} = \begin{bmatrix} x_i \\ y_i \\ z_i \end{bmatrix} \tag{2}$$

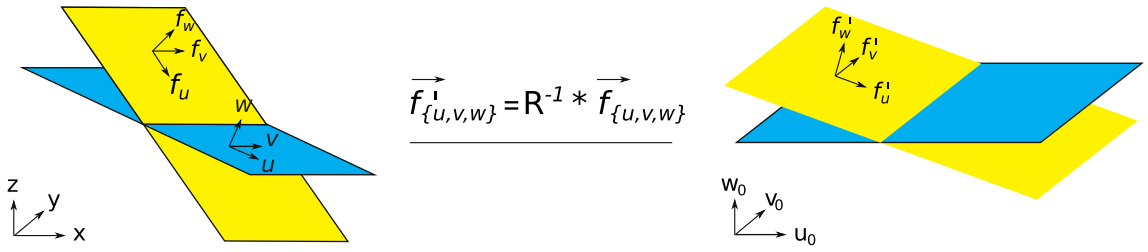

Fig. A.6. The fractures measured on the field are rotated in the (u_0, v_0, w_0) base using the inverse of the rotation matrix R defined by the local stratigraphy orientation. The blue surface represents stratigraphy, while the yellow one represents a fracture. NB: we use trigonometric angles (counterclockwise).

and are computed as follows:

$$\boldsymbol{x}_0 = \begin{bmatrix} 0 \\ 0 \\ 0 \end{bmatrix}, \quad \boldsymbol{x}_1 = \begin{bmatrix} dx_1 \\ dy_1 \\ 0 \end{bmatrix}, \quad \boldsymbol{x}_2 = \begin{bmatrix} dx_2 \\ -dy_2 \\ -dz \end{bmatrix}, \quad \boldsymbol{x}_3 = \begin{bmatrix} dx_1 + dx_2 \\ dy_1 - dy_2 \\ dz \end{bmatrix} \tag{3}$$

with $dx_1 = cos(\alpha) * l$ and $dy_1 = sin(\alpha) * l$ (where $-\alpha$ is the strike of the fracture with respect to the $\boldsymbol{i}$ axis) are the components of $\overrightarrow{\boldsymbol{x}_0\boldsymbol{x}_1}$. $dx_2 = sin(\alpha) * d'$, $dy_2 = cos(\alpha) * d'$, and $dz = sin(\theta)$ are the components of $\overrightarrow{\boldsymbol{x}_0\boldsymbol{x}_2}$ (with $d' = cos(\theta) * d$ and θ the dip of the fracture). Finally $\overrightarrow{\boldsymbol{x}_0\boldsymbol{x}_3} = \overrightarrow{\boldsymbol{x}_0\boldsymbol{x}_1} + \overrightarrow{\boldsymbol{x}_0\boldsymbol{x}_2}$.

2.5. Placement and rotation of the fractures

After the initial fractures are built, they are translated one by one into the 3D model, and then rotated according to the local stratigraphy orientation. Clearly, if a 3D geological model with known structure orientation is not used, this is not possible, and the fractures are kept with their original orientation.

2.5.1. Translation of the fractures inside the model

Let us consider one fracture previously generated. Before moving it, its gravity center $\boldsymbol{c}$ is computed:

$$\boldsymbol{c} = \frac{1}{4}\sum_{i=0}^{3} \boldsymbol{x}_i \tag{4}$$

as well as the lag vectors $\boldsymbol{v}_i$, which are the vectors between the gravity center $\boldsymbol{c}$ and each point $\boldsymbol{x}_i$ of the fracture:

$$\boldsymbol{v}_i = \boldsymbol{x}_i - \boldsymbol{c}. \tag{5}$$

We then use the geology and orientation information obtained from the potential field (here exported from *geomodeller*) in a voxel grid. For every voxel, the information available is a code indicating the geological formation F_f (where $f \in 1, 2, ..., N_F$ with N_F the number of geological formations in the model), and the gradient $\boldsymbol{G}$ of the potential in the voxel. The combination of these 2 pieces of information allows us to define several rules for the generation of the fractures. The first rule is that a given family of fractures will develop only into certain specific formations according to their competence, e.g., the fractures can be generated only in hard rock formations (like limestones or sandstones) but not into soft rocks (shales). This is done by first indexing the voxels that belong to the different formations with an indicator function I_f that is defined for every voxel $\boldsymbol{i} = (i,j,k)$ of the model and for every formation f:

$$I_f(\boldsymbol{i}) = \begin{cases} 1 & \text{if } F(\boldsymbol{i}) = f \\ 0 & \text{if not} \end{cases}. \tag{6}$$

After that, we select randomly one of the cells $\boldsymbol{i_r}$ and test if it is possible to place a fracture in the selected voxel. To speedup the search, the voxels are ordered in a 1D array, from which we randomly select only the valid voxels, i.e., the ones tat can be affected by a given fracture family f. Knowing the origin of the grid $\mathbf{o} = (o_x, o_y, o_z)$, and the dimensions of the cells dx,dy,dz, then a random point $\boldsymbol{x_r}$ is generated inside the cell using a uniform distribution (i.e., the gravity center for the new fracture is found randomly *within the selected voxel*):

$$\boldsymbol{x_r} = \begin{bmatrix} o_x + (j_c - 1)dx + dxrand() \\ o_y + (i_c - 1)dy + dyrand() \\ o_z + (k_c - 1)dz + dzrand() \end{bmatrix} \tag{7}$$

where i_c, j_c, k_c are the matrix indices of the randomly selected cell, and $rand()$ is a random function that generates a random floating point number in the interval [0,1].

Finally, the displacement vector $\boldsymbol{d}$ between $\boldsymbol{c}$ (gravity center of the fracture) and the random point $\boldsymbol{x_r}$ is computed. $\boldsymbol{x_r}$ becomes the new gravity center of the fracture:

$$\boldsymbol{d} = \boldsymbol{x_r} - \boldsymbol{c}. \tag{8}$$

The new points of the fracture $\boldsymbol{x_i'}$ are computed with their respective $\boldsymbol{v_i}$ vectors or by using the displacement vector $\boldsymbol{d}$:

$$\boldsymbol{x_i'} = \boldsymbol{x_r} + \boldsymbol{v_i} = \boldsymbol{x_i} + \boldsymbol{d}. \tag{9}$$

2.5.2. Rotation according to the local geological orientation

After the fracture has been placed into the medium, a rotation is applied to account for the local geological orientation. The rotation of the fracture is made in 3 steps. First a new local orthonormal basis consistent with the orientation of the stratigraphy is built. Secondly, the rotation matrix is computed, and finally every point of the fracture is rotated using this rotation matrix.

In the case of a perfectly cylindrical fold, the components of the new orthonormal basis can be easily computed using the normal vector to stratigraphy, and its dip. But in many cases, a perfectly cylindrical fold is quite rare, and we must consider that it may be tilted, i.e., the fold may present an axial plunge direction. In this case, the new right-handed orthonormal basis ($\boldsymbol{u}$,$\boldsymbol{v}$,$\boldsymbol{w}$) will be as follows:

- $\boldsymbol{w}$, the basis component which corresponds to the normal vector to the stratigraphy
- $\boldsymbol{v}$, the component that corresponds to the plunge direction
- $\boldsymbol{u}$, the component that is orthogonal to the others, and which corresponds to the tilted dip.

This is shown in Fig. A.3.

To compute this basis, the method described in Hillier et al. (2013) is used: using a neighborhood of N neighbors around a given point, the sum of the cross-products of the N normalized normal vectors $\boldsymbol{n}_i$ gives the following pole orientation matrix:

$$\sum_{i=1}^{N} \boldsymbol{n}_i \times \boldsymbol{n}_i^{\mathrm{T}} = \begin{bmatrix} \sum_{i=1}^{N} n_{ix}^2 & \sum_{i=1}^{N} n_{ix}n_{iy} & \sum_{i=1}^{N} n_{ix}n_{iz} \\ \sum_{i=1}^{N} n_{iy}n_{ix} & \sum_{i=1}^{N} n_{iy}^2 & \sum_{i=1}^{N} n_{iy}n_{iz} \\ \sum_{i=1}^{N} n_{iz}n_{ix} & \sum_{i=1}^{N} n_{iz}n_{iy} & \sum_{i=1}^{N} n_{iz}^2 \end{bmatrix}. \tag{10}$$

Then, the eigen vector analysis of this orientation tensor yields eigen values E_1, E_2, and E_3 with $E_1 < E_2 < E_3$ and the eigen vector matrix $\boldsymbol{V}$:

$$\boldsymbol{V} = \begin{bmatrix} e_{1x} & e_{2x} & e_{3x} \\ e_{1y} & e_{2y} & e_{3y} \\ e_{1z} & e_{2z} & e_{3z} \end{bmatrix} \tag{11}$$

with $\boldsymbol{e}_1$, $\boldsymbol{e}_2$, and $\boldsymbol{e}_3$ being the eigen vectors associated with the eigen values E_1, E_2, and E_3. Woodcock (1977) explains that $\boldsymbol{e}_1$ represents the direction for which the inertia momentum is minimized, therefore corresponding to the plunge direction, $\boldsymbol{e}_3$ corresponds to the major momentum of inertia, i.e., to the normal vector to the stratigraphy, and $\boldsymbol{e}_2$ is simply orthogonal to the others. Consequently, we can define $\boldsymbol{u}$, $\boldsymbol{v}$, and $\boldsymbol{w}$ as follows:

$$\boldsymbol{u} = \boldsymbol{e}_2/\|\boldsymbol{e}_2\| \ , \quad \boldsymbol{v} = \boldsymbol{e}_1/\|\boldsymbol{e}_1\| \ , \quad \boldsymbol{w} = \boldsymbol{e}_3/\|\boldsymbol{e}_3\| . \tag{12}$$

The rotation matrix $\boldsymbol{R}$ is then defined as follows:

$$\boldsymbol{R} = [\boldsymbol{u}, \boldsymbol{v}, \boldsymbol{w}]. \tag{13}$$

We can now use this rotation matrix to generate the four rotated vertices of the fracture $\boldsymbol{x}_{ir}'$:

$$\boldsymbol{x}_{ir}' = \boldsymbol{x}_r + \boldsymbol{R}\boldsymbol{v}_i. \quad (14)$$

2.5.3. Results of 3D fracture modeling in a folded environment

Fig. A.4 shows an example of fracture generation with 3 different orientations. One fracture family that is parallel to fold axis (Fig. A.4a) and corresponds to *bc* fracture type in Fig. A.1. The second is perpendicular (Fig. A.4b) and corresponds to *ac* fracture type in Fig. A.1. Fig. A.4c and d shows two conjugate families that correspond to *C1a* and *C1b* fracture types in Fig. A.1.

The rotated fractures reproduce quite well the theoretical orientations of fractures with respect to folds shown in Fig. A.1. Furthermore, fracture orientations follow the orientation and shape of the folds (antiform and synform).

3. Discussion

The present paper shows how an implicit geological model based on the *potential field* (Lajaunie et al., 1997; Calcagno et al., 2008) can be used to generate discrete fracture networks that account for the local orientation of the geological layers. This is especially useful in folded regions. The method is sufficiently versatile to be adapted to any kind of implicit methods, such as the *GeoChron model* (Moyen, 2005; Mallet, 2014) for example. The only requirement is to have access to a 3D field of local orientations.

As it has been shown in the literature (e.g., Mace, 2006; Davy et al., 2013; Bonneau et al., 2013), geomechanical control over the fracture growth, relative position, and interaction are very important. Here, these interactions are not considered because the aim of the paper is to show how the implicit method can be used to rotate the fractures within the structures. Many further improvements could however be considered, including such interactions that would impact the fracture length distribution and the fracture spacing.

One straightforward extension would be to use the implicit model to detect not only the orientation but also the type of fractures that could be expected at a specific location. Indeed, the information provided by the implicit model (potential, gradient, but also curvature) can be used to define the different zones of the fold (intrados, extrados). Fig. A.5 illustrates this idea.

To be more precise, first, the value of the potential $P(\boldsymbol{x})$ for each geological formation f allows defining the position within the layer. For that we suggest, to normalize it as follows (Fig. A.5a):

$$P_f' = \frac{P - P_{f,min}}{P_{f,max} - P_{f,min}} \quad | \quad f \in \{1, \ldots, N_F\} \quad (15)$$

where N_F is the number of geological formations, P_f' is the normalized potential, and $P_{f,min}$ and $P_{f,max}$ are the minimal and maximal values of $P(\boldsymbol{x})$ for the formation f.

Then, the Laplacian of the potential $\Delta\boldsymbol{G}(\boldsymbol{x})$ allows defining the type of fold (syncline or anticline) in the following way (Fig. A.5b):

$$\begin{cases} \text{if } \Delta\boldsymbol{G}(\boldsymbol{x}) > 0 & \text{anticline} \\ \text{if } \Delta\boldsymbol{G}(\boldsymbol{x}) < 0 & \text{syncline} \end{cases}. \quad (16)$$

By combining these two pieces of information, and taking the absolute value $|\Delta\boldsymbol{G}(\boldsymbol{x})|$, one can locate in an approximate manner the zones of maximum deformation within the fold. This principle is illustrated in Fig. A.5c. Such local information could then be used to modify locally the density of the various fracture types. While in theory, the compressive and extensive regimes are expected to be separated roughly by the median line $P_{f'} = 0.5$, further research is needed to propose a reasonable model for the distribution of *fracture seeds* depending on the position and curvature.

Furthermore, the approximation given by the rotation matrix may not reflect the real geomechanical constraints. Producing a more realistic model of conjugate fracture systems would require to establishing further links with geomechanics. Nevertheless, the use of the implicit model proposed here shows that some promising results can be obtained simply and at a low computational cost.

Finally, the use of the implicit method opens a link to structural uncertainty analysis; for example Wellmann et al. (2010) show the use of an uncertainty analysis on the geological model, and Lindsay et al. (2013) include also geophysical observations in the inverse framework. As the geological structure (i.e., the geological model) has a deep impact on the subsequent DFN model, it would make sense to combine both steps in the same uncertainty analysis. Cherpeau et al. (2012) uses an implicit method to simulate faults in a Monte Carlo Markov Chain framework. A similar approach could be imagined for DFNs.

4. Conclusions

In this paper, we propose a methodology allowing us to use the information provided by an implicit geological model about the deformation within a folded structure to generate oriented discrete fracture networks (DFN). The methodology is simple: the gradient of the potential is extracted from the implicit model. It is used to rotate the fractures within the fold. The fracture sets can either be taken from a theoretical model such as Twiss and Moores (1992) or provided by the user. For the length distribution, the code can use several user-defined distribution laws. The resulting DFN models can be rasterized if needed for further use in any subsequent modeling applications.

Several possible further improvements are discussed such as the addition of "geomechanical rules" to better account for the position of the fractures within the structure. This would allow simulating the different fracture families within specific zones of the fold (compression in the intrados and extension in the extrados).

Acknowledgments

Part of the funding of this work was provided by Schlumberger Water Services.

Appendix A. Consideration and integration of field data in the proposed approach

One option with the model is to reproduce fracture families that are observed in the field. The classical approach consists in using the same orientation anywhere in the domain and this is feasible with the code.

However, a more interesting option consists in analyzing the field data in relation with the local orientation of the strata. This allows us to obtain families that are independent of the position in the complex 3D setting. These families are then used in the procedure described in the paper.

To analyze the field observations, we proceed as follows: the observed fractures are *rotated* into the local coordinate system ($\boldsymbol{u}_0$, $\boldsymbol{v}_0$, $\boldsymbol{w}_0$) derived either from the 3D geological model as explained in the paper, or from local analysis of the orientation of the stratigraphy as explained in Hillier et al. (2013). This is then done using the inverse of the rotation

matrix R defined by the local stratigraphy orientation defined in Eq. (13) (Fig. A.6). The fracture plane system ($\boldsymbol{f_u}, \boldsymbol{f_v}, \boldsymbol{f_w}$) is transformed in a *reference* system ($\boldsymbol{f_{u'}}, \boldsymbol{f_{v'}}, \boldsymbol{f_{w'}}$) as follows:

$$\boldsymbol{f'_u} = \boldsymbol{R^{-1}} \boldsymbol{f_u} \ , \quad \boldsymbol{f'_v} = \boldsymbol{R^{-1}} \boldsymbol{f_v} \ , \quad \boldsymbol{f'_w} = \boldsymbol{R^{-1}} \boldsymbol{f_w} . \tag{A.1}$$

Using this procedure, all the fractures measured in the field are *normalized* accounting for the local orientation of the bedding. This transformed dataset allows computing fracturation statistics independently from the orientation of the stratigraphy.

References

Ackermann, R.V., Schlische, R.W., Withjack, M.O., 2001. The geometric and statistical evolution of normal fault systems: an experimental study of the effects of mechanical layer thickness on scaling laws. J. Struct. Geol. 23 (11), 1803–1819.

Bazagette, L., 2004. Relations plissement/fracturation multi échelle dans les multicouches sédimentaires du domaine élastique/fragile: accommodation discontinue de la courbure par la fracturation de petite échelle et par les articulations. possibles implications dynamiques dans les écoulements des réservoirs. (Ph.D. thesis). Université de Montpellier II, France.

Bellahsen, N., Fiore, P., Pollard, D., 2006. The role of fractures in the structural interpretation of Sheep mountain anticline, Wyoming. J. Struct. Geol. 28 (5), 850–867.

Bonneau, F., Henrion, V., Caumon, G., Renard, P., Sausse, J., 2013. A methodology for pseudo-genetic stochastic modeling of discrete fracture networks. Comput. Geosci. 56, 12–22.

Borghi, A., Renard, P., Jenni, S., 2012. A pseudo-genetic stochastic model to generate karstic networks. J. Hydrol. 414–415 (0), 516–529.

Bour, O., Davy, P., Darcel, C., Odling, N.E., 2002. A statistical scaling model for fracture network geometry, with validation on a multiscale mapping of a joint network (Hornelen basin, Norway). J. Geophys. Res. 107 (B6), 2113.

Calcagno, P., Chilès, J., Courrioux, G., Guillen, A., 2008. Geological modelling from field data and geological knowledge: Part i. modelling method coupling 3d potential-field interpolation and geological rules. Phys. Earth Planet. Inter. 171 (1–4), 147–157 (recent Advances in Computational Geodynamics: Theory, Numerics and Application).

Caumon, G., Gray, G., Antoine, C., Titeux, M.-O., 2013. Three-dimensional implicit stratigraphic model building from remote sensing data on tetrahedral meshes: theory and application to a regional model of la popa basin, ne Mexico. IEEE Trans. Geosci. Remote Sens. 51 (3), 1613–1621 (March).

Cherpeau, N., Caumon, G., Caers, J., Lévy, B., 2012. Method for stochastic inverse modeling of fault geometry and connectivity using flow data. Math. Geosci. 44 (2), 147–168.

Chilès, J.-P., 2005. Stochastic modeling of natural fractured media: a review. In: Leuangthong, O., Deutsch, C.V. (Eds.), Geostatistics Banff 2004. Vol. 14 of Quantitative Geology and Geostatistics. Springer, Netherlands, pp. 285–294 http://dx.doi.org/10.1007/978-1-4020-3610-1_29.

Cowan, E.J., Beatson, R.K., Ross, H.J., Fright, W.R., McLennan, T.J., Evans, T.R., Carr, J.C., Lane, R.G., Bright, D.V., Gillman, A.J., Oshust, P.A., Titley, M., 2003. Practical implicit geological modeling. In: Dominy, S. (Ed.), Proc. 5th International Mining Conference. Australian Inst. Mining and Metallurgy, pp. 89–99.

Davy, P., Le Goc, R., Darcel, C., Bour, O., De Dreuzy, J.-R., Munier, R., 2010. A likely universal model of fracture scaling and its consequence for crustal hydromechanics. J. Geophys. Res. B Solid Earth 115 (B10411).

Davy, P., Le Goc, R., Darcel, C., 2013. A model of fracture nucleation, growth and arrest, and consequences for fracture density and scaling. J. Geophys. Res. Solid Earth 118 (4), 1393–1407.

Dershowitz, W., Pointe, P.L., Doe, T.W., 2004. Advances in discrete fracture network modeling. US EPA/NGWA Fractured Rock Conference, Portland, Maine, USA.

Frank, T., Tertois, A.-L., Mallet, J.-L., Jul. 2007. 3D-reconstruction of complex geological interfaces from irregularly distributed and noisy point data. Comput. Geosci. 33 (7), 932–943.

Freudenreich, Y., Monte, A.A.D., Angerer, E., Reiser, C., Glass, C., 2005. Fractured reservoir characterisation from seismic and well analysis: a case study. 67th EAGE Conference and Exhibition, Madrid Spain.

Geomodeller3D, 2013. Editeur geologique 3d. INTREPID Geophysics. URL. http://www.geomodeller.com.

Hillier, M., de Kemp, E., Schetselaar, E., 2013. 3d form line construction by structural field interpolation (SFI) of geologic strike and dip observations. J. Struct. Geol. 51, 167–179.

Jing, L., 2003. A review of techniques, advances and outstanding issues in numerical modelling for rock mechanics and rock engineering. Int. J. Rock Mech. Min. Sci. 40 (3), 283–353.

Kloppenburg, A., Alzate, J.C., Charry, G.R., 2003. Building a discrete fracture network based on the deformation history: a case study from the Guaduas field, Colombia. VIII Simposio Bolivariano — Exploracion Petrolera en las Cuencas Subandinas.

La Pointe, P., Hudson, J.A., 1985. Characterization and interpretation of rock mass joint patterns. Special Paper/Geological Society of, America 199, pp. 1–38.

Lajaunie, C., Courrioux, G., Manuel, L., 1997. Foliations field and 3d cartography in geology: principles of a method based on potential interpolation. Math. Geol. 29, 571–584.

Lindsay, M.D., Perrouty, S., Jessell, M.W., Aillères, L., 2013. Making the link between geological and geophysical uncertainty: geodiversity in the Ashanti greenstone belt. Geophys. J. Int. ggt311.

Mace, L., 2006. Caractérisation et modélisation numérique tridimensionnelle des réseaux de fractures naturelles. (Ph.D. thesis). INPL, Nancy, France.

Maerten, L., Pollard, D.D., Karpuz, R., 2000. How to constrain 3-d fault continuity and linkage using reflection seismic data: a geomechanical approach. AAPG Bull. 84 (9), 1311–1324.

Mallet, J.-L., 2014. Elements of Mathematical Sedimentary Geology: The GeoChron Model. EAGE Publications.

Moyen, R., 2005. Paramétrisation géo-chronologique. (Ph.D. thesis). INPL, Nancy, France.

Moyen, R., Mallet, J.-L., Frank, T., Leflon, B., Royer, J.-J., 2004. 3d-parameterization of the 3d geological space — the geochron model. 9th European Conference on the Mathematics of Oil Recovery. EAGE.

Odling, N., 1997. Scaling and connectivity of joint systems in sandstones from western Norway. J. Struct. Geol. 19 (10), 1257–1271.

Olson, J., 1993. Joint pattern development: effects of subcritical crack growth and mechanical crack interaction. J. Geophys. Res. 98 (B7), 12251–12265.

Price, N., 1966. Fault and joint development in brittle and semi-brittle rock vol. 1. Pergamon Press, London.

Price, N., Cosgrove, J., 1990. Analysis of Geological Structures. Cambridge University Press.

Priest, S., 1993. Discontinuity Analysis for Rock Engineering. Springer, Netherlands.

Priest, S.D., Hudson, J.A., 1981. Estimation of discontinuity spacing and trace length using scanline surveys. Int. J. Rock Mech. Min. Sci. Geomech. Abstr. 18 (3), 183–197.

Sassi, W., Guiton, M., Leroy, Y., Daniel, J., Callot, J., 2012. Constraints on bed scale fracture chronology with a fem mechanical model of folding: the case of split mountain (Utah, USA). Tectonophysics 576, 197–215.

Soliva, R., Benedicto, A., 2005. Geometry, scaling relations and spacing of vertically restricted normal faults. J. Struct. Geol. 27 (2), 317–325.

Souche, L., Lepage, F., Iskenova, G., 2013. Volume based modeling-automated construction of complex structural models. 75th EAGE Conference & Exhibition Incorporating SPE EUROPEC 2013.

Twiss, R., Moores, E., 1992. Structural Geology. W.H. Freeman.

Wellmann, J.F., Horowitz, F.G., Schill, E., Regenauer-Lieb, K., 2010. Towards incorporating uncertainty of structural data in 3d geological inversion. Tectonophysics 490 (3–4), 141–151.

Woodcock, N., 1977. Specification of fabric shapes using an eigenvalue method. Geol. Soc. Am. Bull. 88 (9), 1231–1236.

Zahm, C., Hennings, P.H., 2009. Complex fracture development related to stratigraphic architecture; challenges for structural deformation prediction, tensleep sandstone at the Alcova anticline, Wyoming. AAPG Bull. 93, 1427–1446.